

Interactively Full-Color Changeable Electronic Fiber Sensor with High Stretchability and Rapid Response

Yunpeng Wang, Wenbin Niu,* Chiao-Yueh Lo, Yusen Zhao, Ximin He, Guorui Zhang, Suli Wu, Benzhi Ju, and Shufen Zhang

Smart interactive electronic devices can dynamically respond to and visualize environmental stimuli. Inspired by the rapid color changes of natural creatures, an interactive electronic fiber sensor with high stretchability and tunable coloration is presented. It is based on an ingenious multi-sheath design on a piezoresistive electronic fiber coupled with a mechanochromic photonic crystal microtubule. It has the unique capabilities of sensing and visualizing its deformation simultaneously, by reconstructing conductive paths and regulating the lattice spacing of the photonic sheath. In particular, it exhibits dynamic color switching spanning the full visible region (from red to blue), fast optical/electrical response (≈ 80 ms), and a large working range (0–200%), allowing its application as a user-interactive sensor for dynamically monitoring large joint movements and muscle microvibrations of the human body in real time. This investigation provides a general platform for emerging interactive devices, which are promising for applications in wearable electronics, human–machine interactions, and intelligent robots.

1. Introduction

The increasingly diverse and complex requirements of modern electronic devices have motivated the rapid development of stretchable and wearable electronics. These electronic devices are capable of converting external stimuli into measurable electrical signals (e.g., resistance,^[1] capacitance,^[2] and electricity^[3]), which plays a vital role in the fields of human activity monitoring, personal health management, electronic skin, soft robots, and artificial limbs.^[4] In particular, for realizing the direct intelligent interaction between users and devices, a series of interactive electronic devices have been realized by combining electronic sensors with human-readable visual readouts. Apart from having accurate electrical response signals, they can

also visually identify, monitor, and quantify stimulus sources simultaneously.^[5] For example, flexible interactive sensors based on light-emitting devices (such as organic light-emitting diodes,^[6] polymeric light-emitting devices,^[7] and inorganic phosphors^[8]) have demonstrated the ability to quantify pressure or strain via changes in brightness, possessing high spatial and temporal resolution and instantaneous visual response properties.^[6a,b,8a] Unfortunately, the brightness perceived by naked eyes is greatly affected by ambient light, reducing the accuracy of visual information acquiring. In addition, human eyes are not sensitive enough to brightness change in order to directly read out the strain or pressure applied to the device. To this end, the introduction of color-changing elements is necessary for interactive displays in view of human's better sensitivity to color perception. However,

current colorimetric sensors (e.g., electrochromic dyes,^[9] thermochromic dyes,^[5a,10] and mechanochromic dyes^[11]) are subject to low brightness and low response speed due to inherent limitations of those chromic dyes.^[5a,6b] Moreover, those dyes can switch between only two color states, leading to relatively low-contrast and low-resolution visual interaction.^[5a,6b] Therefore, it is still a great challenge to develop interactive wearable devices with brilliant, rapid, and wide color-switching ranges in the full visible region. A combination of rational mechanochromic materials and the design of geometric structures would be an effective strategy to realize this goal.

Here, we present a novel interactive sensor by integrating a photonic crystal with tunable structural colors in the entire visible spectrum into an electronic fiber to provide a visual information display, as shown in **Figure 1**. In nature, brilliant structural colors produced by periodic microstructures based on photonic crystals play an irreplaceable role in many organisms, such as chameleons,^[12] squids,^[13] cuttlefishes,^[14] tropical fishes,^[15] insects,^[16] and peacocks.^[17] They can actively regulate these microstructures to change colors for reproduction, camouflage, display, and communication.^[12,17,18] This unique phenomenon has inspired the rapid development of photonic materials that respond to external stimuli such as mechanical force,^[19] solvent,^[20] temperature,^[21] light,^[22] etc. Among them, highly stretchable mechanochromic photonic crystal materials have great potential in developing next-generation user-interactive wearable devices because they can respond to strain with

Dr. Y. Wang, Prof. W. Niu, G. Zhang, Prof. S. Wu, Prof. B. Ju, Prof. S. Zhang
State Key Laboratory of Fine Chemicals
Dalian University of Technology
West Campus, 2 Linggong Rd., Dalian 116024, China
E-mail: niuw@dlut.edu.cn

Dr. C.-Y. Lo, Dr. Y. Zhao, Prof. X. He
Department of Materials Science and Engineering
University of California
Los Angeles, CA 90095, USA

 The ORCID identification number(s) for the author(s) of this article can be found under <https://doi.org/10.1002/adfm.202000356>.

DOI: 10.1002/adfm.202000356

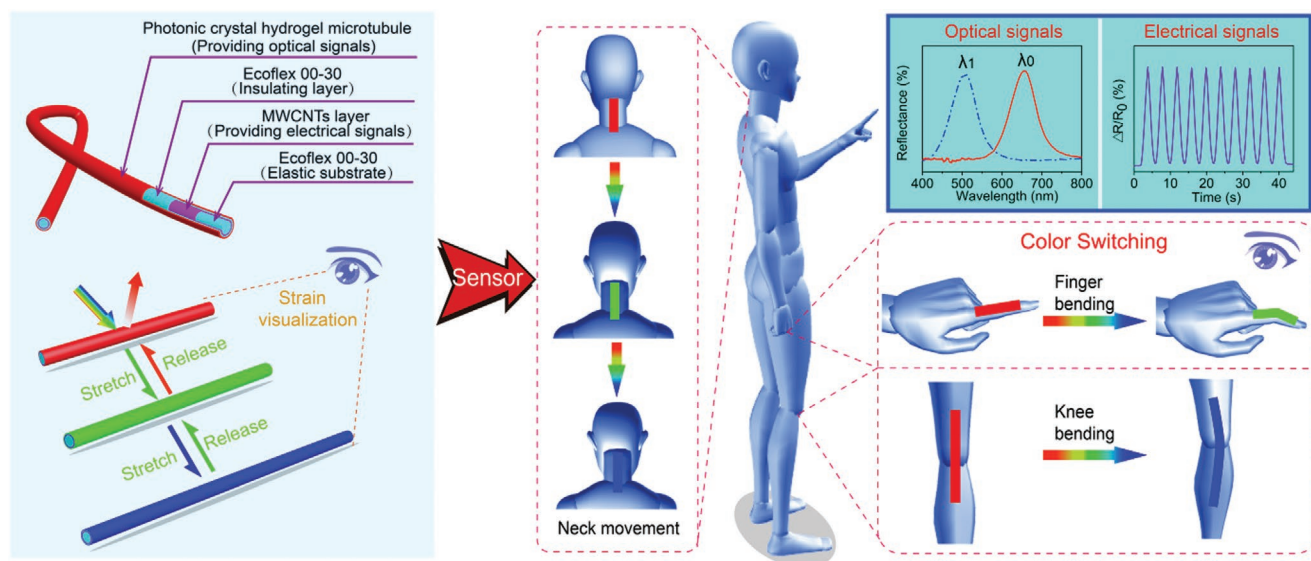


Figure 1. Conceptual illustration of interactively full-color changeable electronic fiber sensor.

panchromatic transformation, and thus generate direct feedback to human eyes.^[23]

In this paper, we report the rational design and fabrication of interactively tunable full-color electronic fiber sensors with high stretchability, rapid optical/electrical response, and dynamic color switching. As shown in Figure 1, we first designed and manufactured a stretchable photonic crystal hydrogel hollow microtubule as an optical sensing element. Such a hollow photonic microtubule has rarely been reported. Then, a bi-sheath piezoresistive fiber was fabricated by coating a silicone core with multiwall carbon nanotubes (MWCNTs) layer and silicone insulating layer, respectively. Subsequently, this piezoresistive fiber was coupled with the photonic microtubule to form a multisheath interactive fiber sensor. When we stretch the sensor (from 0% to 200%), the electrical readout originating from the piezoresistive fiber deformation can be recorded accurately by electrical instruments, which in turn serves as an indicator to precisely quantify the deformation. Simultaneously, the photonic crystal undergoes instantaneous and reversible color changes throughout the visible region, and directly feedback strain information to human to achieve the interactive function of device. Moreover, the color change of the microtubule does not require electrical or thermal energy to drive it; thus, this microtubule is an ideal low-power material. As a wearable user-interactive device, our full-color changeable electronic fiber can be used to real-time track various human movements.

2. Results and Discussion

2.1. Preparation and Mechanochromic Properties of the Stretchable Photonic Crystal Microtubule

The photonic crystal microtubule is composed of several thousands of rigid poly(dodecylglyceryl itaconate) (PDGI) lamellar bilayers (thickness, ≈ 4.7 nm) stacked periodically in a chemically crosslinked poly(acrylamide) (PAAm) hydrogel network.^[24]

The fabrication process of PDGI photonic crystal microtubule is depicted in Figure 2a. Dodecylglyceryl itaconate (DGI) was self-assembled into bilayer membranes stacked periodically in an aqueous solution, containing acrylamide (AAM), sodium dodecyl sulfate (SDS), the crosslinker *N,N*'-methylenebis acrylamide (MBAA), and a photoinitiator. The DGI bilayers were aligned under shear force by injecting the above precursor into a tube-like template.^[25] Then, periodically stacked DGI bilayers were polymerized and entrapped in PAAm network.^[26] Finally, the PDGI photonic crystal microtubule was obtained by swelling in deionized water. The structural color of the microtubule before swelling was blue (Figure 2b). During the swelling process, the distance d between PDGI bilayers (thickness of PAAm layer) increased from d_1 to d_2 ($d_1 < d_2$), and a redshift in structural color can be observed (Figure 2a).^[24b] As shown in Figure 2c and Figure S1 in the Supporting Information, the cross-sectional scanning electron microscopy (SEM) images of PDGI and pure PAAm hydrogel (without PDGI) were remarkably different. The PDGI hydrogel showed a separated phenomenon, indicating that PDGI bilayer membranes were indeed fixed in PAAm network in a layered arrangement.^[27]

A series of PDGI microtubules with distinct structural colors were prepared by adjusting crosslinker MBAA concentration and template size. According to Bragg's diffraction Equation (1)

$$m\lambda = 2nd \sin \theta \quad (1)$$

where m is the order of diffraction, λ represents the reflection wavelength, n is the effective refractive index, d is the lattice spacing, and θ refers to the incident angle.^[24b] The reflection wavelength of the photonic microtubule is governed by the spacing between PDGI bilayers (d) in this case (Figure S2, Supporting Information), whereas the crosslink density of the PAAm network determines the swelling degree of the hydrogel and thus the spacing d .^[28] Specifically, the higher the crosslink density, the smaller the swelling behavior and layer spacing d . Therefore, by controlling the spacing d of the PDGI bilayers

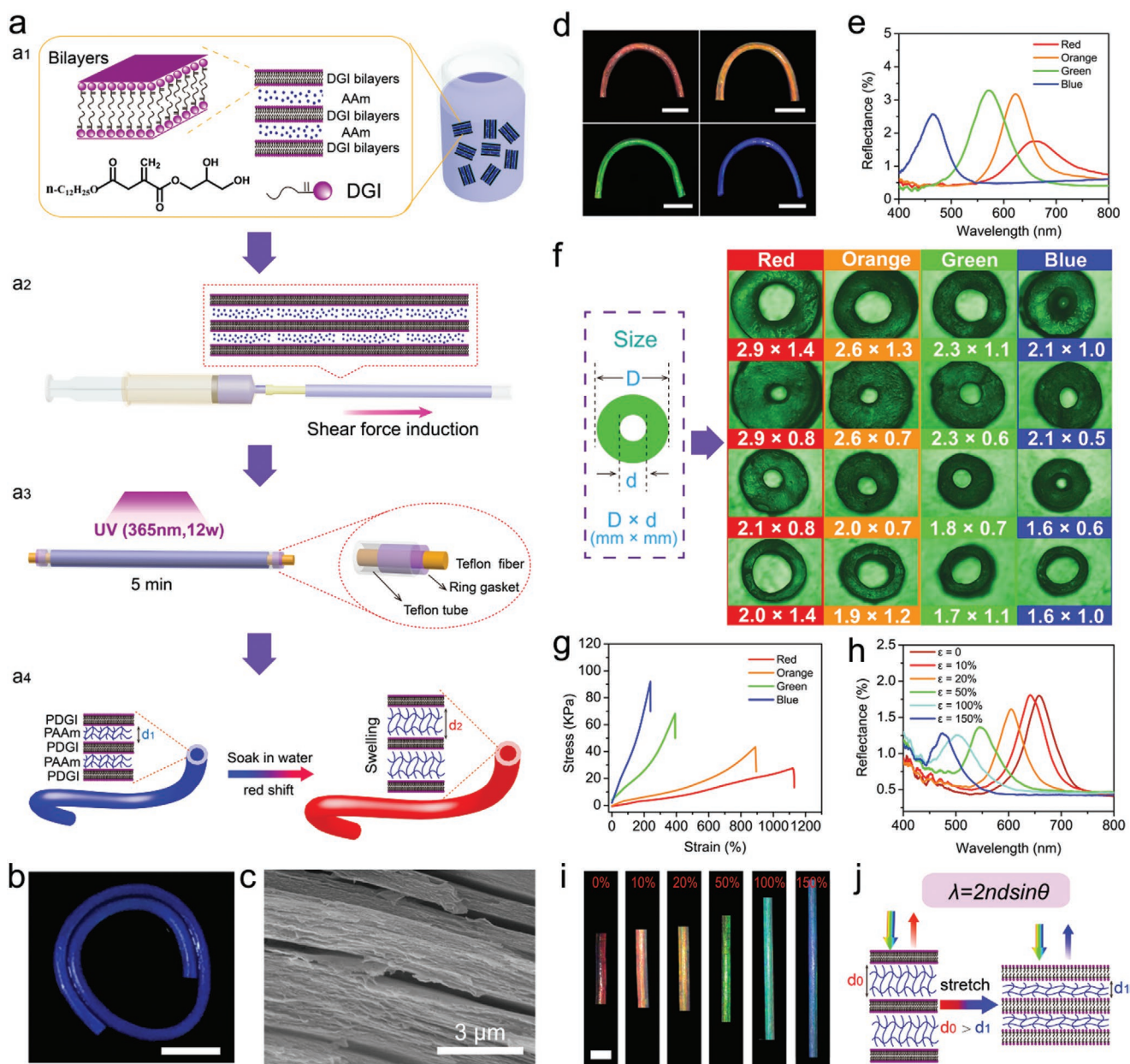


Figure 2. a) Schematic illustration of the fabrication process of PDGI photonic crystal hydrogel microtubule. b) Optical images of PDGI microtubule before swelling. Scale bar is 1 cm. c) Cross-sectional SEM image of PDGI microtubule. d) Optical images of PDGI microtubule (after swelling) with different structural colors obtained by adjusting MBAA concentration. Scale bar is 1 cm. e) Reflectance spectra of the samples in (d). f) Cross-sectional images of photonic microtubules with different specifications taken through an optical microscope. g) Stress–strain curves of PDGI photonic microtubules with different structural colors, showing stiffer behavior and blue color for high crosslinking, while softer and red color for low crosslinking. h) Reflectance spectra of microtubule (with an initial reflection wavelength of 657 nm) under various strains, and i) the corresponding photographs. Scale bar is 0.5 cm. j) Mechanism illustration of the blueshift phenomenon of structural color during stretching.

via the MBAA concentration, we successfully fabricated PDGI microtubules with brilliant structural colors covering the whole visible region (from red, to orange, green, and blue) (Figure 2d). As shown in Figure 2e, the reflection wavelength ranges from 660 to 464 nm as the crosslinker amount increases from 2 to 16 mg (Table S1 and Figure S3, Supporting Information). After the PDGI photonic microtubule was immersed in water for 1 day to reach the swelling equilibrium, its maximum reflection peak would remain almost unchanged in water

(Figure S4, Supporting Information). This is because of the hydrogen bonding between PDGI and PAAm, ensuring that PDGI does not escape from the gel network. This stable structure gives the gel a durable structural color. Moreover, a variety of PDGI microtubules with different outer and inner diameters were also prepared by adjusting the size of the templates. Figure 2f shows cross-sectional optical micrographs of those PDGI microtubules. The outside diameters (D) decreased as the color of the microtubules changed from red to blue due to

the differences of their swelling degrees, as shown in the rows. Correspondingly, by facilely manipulating the template specifications, various photonic microtubules with different sizes could be fabricated, as shown in the columns.

Additionally, the as-prepared photonic microtubules exhibit excellent tensile properties because the hard PDGI bilayer embedded in PAAM network provides reversible sacrificial bonds (Figure 2g).^[29] Specifically, the tensile fracture strain of the blue PDGI microtubule reached $\approx 200\%$ with a fracture strength of ≈ 92 kPa, and the red PDGI microtubule shows a notable tensile fracture strain up to $\approx 1100\%$ but a decreased fracture strength of ≈ 28 kPa. We attribute this tensile behavior difference to the different crosslink density of the hydrogel networks.^[30] Increasing the crosslink density would enhance the interaction between polymer segments inside the hydrogel, thus restricting chain movement and leading to the enhancement in their mechanical strength.^[31] Remarkably, the structural color of the photonic microtubules is responsive to mechanical stimuli and has excellent reversibility. The structural color immediately returns to its initial state once the stress is removed (Movie S1, Supporting Information). The red photonic microtubule achieves reversible and dynamical color switching within full visual region from red at 657 nm to blue at 473 nm as the applied strain increased from 0% to 150%, as displayed in Figure 2h,i. This color switching phenomenon can be explained by the Bragg formula: the bilayer spacing d is reduced from d_0 to d_1 during stretching, thus resulting in a decrease in λ and a blueshift in the structural color. Such color switching can be visually perceived by human eyes and interacts directly with observers, implying their potential application in interactive wearable devices/electronics.

2.2. Preparation and Mechanoelectrical Performance of Ultrastretched Bi-Sheath Piezoresistive Fibers

Piezoresistive electrically responsive fibers were prepared by loading MWCNTs onto the elastic silicone fiber (Ecoflex 00-30). The preparation process is shown in Figure 3a and Figure S5 in the Supporting Information. The MWCNTs would adhere to the surface of a swollen silicone fiber through van der Waals forces and entangle with each other to form a conductive network layer (Figure 3b).^[32] Then, the fiber was deswollen in air and shrank in volume, which resulted in the formation of a dense MWCNTs network with small resistance (Figures S6 and S7a, Supporting Information). Eventually, a bi-sheath piezoresistive (Ecoflex/MWCNTs/Ecoflex, EME) fiber was obtained after being coated with a layer of silicone Ecoflex. The silicone acts as both a protective layer and an insulating layer to prevent MWCNTs from detaching during fiber stretching and to avoid short-circuiting in the subsequently constructed device, respectively. Furthermore, EME fibers with distinct electrical response properties were obtained by tuning the MWCNTs dispersion concentration and the number of dip-coating cycles. As shown in Figure 3d and Figure S7 in the Supporting Information, the resistance of EME fibers decreases upon increasing the MWCNTs dispersion concentration from 1 to 2 wt% or the number of dip-coating cycles from 1 to 3 owing to gradually enhanced conductive networks.^[33] A further increase in the

MWCNTs concentration or number of dip-coating cycles led to the MWCNTs precipitating from the dispersion or detaching from the fiber surface (Figure S8, Supporting Information), respectively. Figure 3d shows that the introduction of insulating layer slightly increases the resistance of the sample because the silicone precursor permeates into the MWCNTs conductive network and blocks charge transportation.^[34] For example, among the prepared samples, the sample obtained after dip-coating the fiber in 2 wt% MWCNTs dispersion three times shows a resistance of 0.47 k Ω , and the introduction of insulating layer slightly increases the resistance to 0.87 k Ω .

Figure 3e and Figure S9 in the Supporting Information show the relative resistance change curves ($\Delta R/R_0 = (R - R_0)/R_0$, where R is the measured resistance and R_0 is the initial resistance) as a function of strain. It can be seen that the relative resistance increases progressively during stretching, because the gradual slipping and disconnection between MWCNTs destroy conductive paths, as evidenced in Figure 3g,h and Figure S10 in the Supporting Information.^[32,33b,35] The EME fiber exhibits gauge factor ($GF = (\Delta R/R_0)/\epsilon$, where ϵ denotes the strain) of 24.2 and 76.5 in the strain range of 0–300% and >300%, respectively. Furthermore, the GF of samples can be controlled by adjusting the concentration of MWCNTs dispersion and the number of dip-coating cycles (Figure S11, Supporting Information).^[33b,35,36] On the other hand, the stress–strain curve indicated that the tensile fracture strain of EME fiber was $\approx 550\%$ (Figure 3f; Figure S9, Supporting Information), which was less than that of pure Ecoflex silicone elastomer (>900%).^[32] This is because the rigid structure of MWCNTs conductive network reduces the stretchability of the Ecoflex silicone layer (Figure S12, Supporting Information).^[37] Nevertheless, the excellent intrinsic elasticity of silicone Ecoflex and integrated structure (Ecoflex/MWCNTs/Ecoflex) ensures that the conductive network returns to the original position without buckling,^[33b] thus enabling the resistance to be restored to its initial value. Therefore, our EME fiber has excellent reliability, repeatability, and durability, which are essential in practical application. The relative resistance change was measured to remain almost constant during 15 000 stretching/releasing cycles at 75% strain (Figure S13, Supporting Information), indicating its long service life and value to practical applications.

2.3. Preparation and Interactive Performance of the Full-Color Changeable Electronic Fiber Sensor

As a proof-of-concept experiment, we constructed a novel interactively full-color changeable electronic fiber strain sensor, which enabled interaction and read-out that can be visualized by human eyes via integrating the mechanochromic PDGI photonic microtubule with the piezoresistive EME fiber. Due to the blueshifting of fiber-reflected light under strain, the red PDGI photonic crystal microtubule was employed as the material of the sheath to maximize the color change range within visible region. To achieve high GF, the bi-sheath EME fiber prepared with 3 dip-coating cycles in a 2 wt% MWCNTs dispersion served as the electrically responsive inner core. Figure 4a and Figure S14 in the Supporting Information show the fabrication process of interactive full-color changeable multisheath

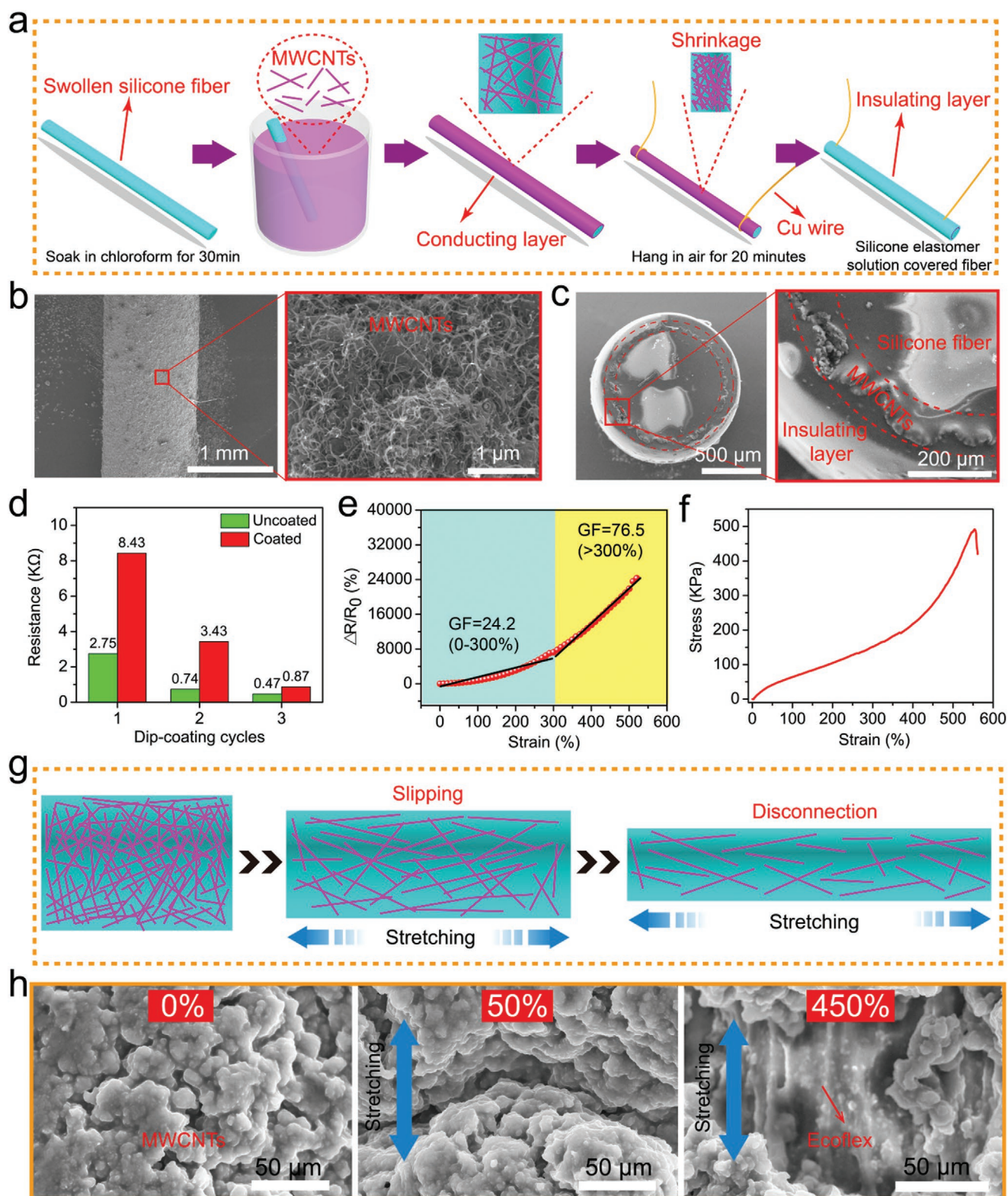


Figure 3. a) Schematic illustration showing the fabrication process of the bi-sheath EME fiber. b) Surface SEM images of the fiber loaded with MWCNTs. c) Cross-sectional SEM images of the EME fiber. d) Resistance values of the EME fibers with different dip-coating cycles in 2 wt% MWCNTs dispersion before and after insulating layer. The length of tested samples is 1 cm. e) Relative resistance change of EME fiber as a function of strain. EME fiber was prepared by dip-coating for 3 cycles in 2 wt% MWCNTs dispersion. f) Stress–strain curves of the EME fiber. g) Schematic diagram and h) the corresponding SEM images showing the change of conductive layer during stretching.

(PDGI/EME, PE) fiber strain sensor. The above EME fiber was inserted into the PDGI microtubule, followed by adhering with ethyl cyanoacrylate adhesive. To ensure close contact and thus the synchronous change in optical and electrical signals, the diameter of the EME fiber equals the inner diameter of the PDGI microtubule. Figure 4b shows that the curves of the relative resistance and reflection wavelength of PE sensor as a function of strain under cyclic stretching/releasing. It is revealed that the sensor exhibit a large strain working range from 0% to 200%. When we stretch/release the sensor, its relative resistance can vary reversibly, providing an electrically detectable signal. A slight hysteresis in the relative resistance was observed due to the viscoelasticity of the silicone elastomer (Figure S15, Supporting Information).^[32] Simultaneously, the reflection wavelength and corresponding structural color change reversibly, dynamically and continuously over the entire visible spectrum (from 632 to 439 nm) with a sensitivity of $\approx 1 \text{ nm}\%$, as intuitively displayed in Figure 4c, indicating high sensitivity and resolution.^[9,11] Compared with the reported interactive sensors with two color states based on chromic dye,^[5a,9,11] our sensor can visualize various strains and feed back to human via continuous full-color change, thus realizing intelligent interaction between users and devices within a large working range (Movie S2, Supporting Information). High sensitivity and high resolution will ensure that the sensor has excellent electrical response and visual readout when monitoring large or tiny movements. Notably, the relative resistance and the reflection wavelength change synchronously, stably, and repeatedly as shown in Figure 4d. Thus the electrical signal, applied strain, and the color of sensor can be accurately correlated. Moreover, the interactive fiber sensor exhibited a rapid response rate of $\approx 80 \text{ ms}$ for electrical and optical signals with strain from 0% to 20% (Figure 4e). The above response time indicated that our sensor is indeed much faster than organic electrochromic (1.4 s),^[9] thermochromic (0.8 s),^[5a] and mechanochromic (2 s)^[11] interactive sensors reported recently. This fast response capability will benefit the real-time monitoring of complicated physical and physiological activities, such as joint bending, breathing, eye opening and closing, and muscle tremors. Figure 4f shows the frequency-dependent electrical response signal. The relative resistance only increases slightly as the frequency increases from 0.05 to 1 Hz at 100% strain. Such a low frequency-dependence reveals that the sensor is suitable for human activity detection at different frequencies.

In addition to the maximum reflection wavelength shift or structural color, the intensity change at the initial maximum reflection wavelength can also be used as an optical indicator for real-time monitoring. As shown in Figure 4g,h, the maximum reflection wavelength of the sensor shifts from 654 to 573 nm when 30% strain is applied, while the optical reflective intensity at 654 nm decreases correspondingly. Note that this variation in optical intensity is also reversible, repeatable, and synchronized with the relative resistance change during cyclic stretching/releasing, as shown in Figure 4i. Furthermore, the optical intensity also exhibits excellent fast response capability with a response time of less than 120 ms at 30% strain (Figure S16, Supporting Information). Therefore, the optical intensity at the initial maximum reflection wavelength can be used as another indicator for the real-time monitoring of the device.

2.4. Diverse Applications of the Interactive Sensor in Human Movement Detection

The outstanding performance of the interactively full-color changeable electronic fiber sensor allowed it to be used as a skin-attachable wearable device for interactive real-time human motion monitoring of different parts of the body (Figure 5a). When body have a movement, the resistance and light amplitude changes could be easily converted into and precisely recorded as digital signals by instruments, while the color change enables intuitive perception by human eyes. In turn, these signals reflect the motion state and quantify the deformation. As a proof-of-concept, the sensor was attached to a finger undergoing bending/unbending cycles, and the electrical and optical signals were observed to vary concurrently (Figure 5b). Notably, the consistency of the signal changes during multiple cycles indicates excellent stability and repeatability, and the structural color switches from red to green, indicating visualizable user-interaction capability. Figure 5c,d displays the relative resistance and light reflection intensity of the sensor in response to repeated bending of elbow and knee joints, respectively. Similarly, stable signal response and color-switching caused by elbow and knee joint motions were also displayed. These results implied that the sensor has an excellent ability to interactively detect large deformation motions of the human body. Figure 5e shows the response of sensor to wrist bending, in which the sensor was fixed to the wrist with hand initially bending upward. These results reveal that the deformation magnitude of the human body could be easily recognized via instruments and captured by the naked eye to visualize the strain. Similar measurement results were also observed in monitoring stepwise neck movements. A stepwise increasing resistance output as well as a stepwise structural color change (from red to green) of the sensor were observed in accordance with the stepwise-increased neck bending angle. Correspondingly, a stepwise structural color change (from red to green) was also shown. In particular, the relative resistance and optical characteristics remain stable when the neck was in a determined state (Figure 5f).

Last but not least, we have also demonstrated that our sensor is sensitive enough to recognize small movements of human body. As shown in Figure 5g,h, our device is capable of recording and reflecting the small facial muscle movements during mouth opening and closing as well as eye blinking. Figure 5i displays the performance of our device on tracking abdominal movement during respiration, and it is successful in distinguishing a normal breath and a deep breath by their distinct peak amplitudes. Specifically, during a normal breath, the signals changed stably and shallowly, while stronger signal peaks were shown during a deep breath. Moreover, as shown in Figure S17 in the Supporting Information, the slight arm muscle vibration behavior during clenching was detected and recorded apparently by the corresponding signals. Compared with the aforementioned results under large body deformations, smaller color-changing range was visualized under small strain movements. The significant color change in various body-motion sensors revealed that the deformation magnitude of human body could not only be easily recognized via instruments but also be perceived intuitively by naked eyes, enabling

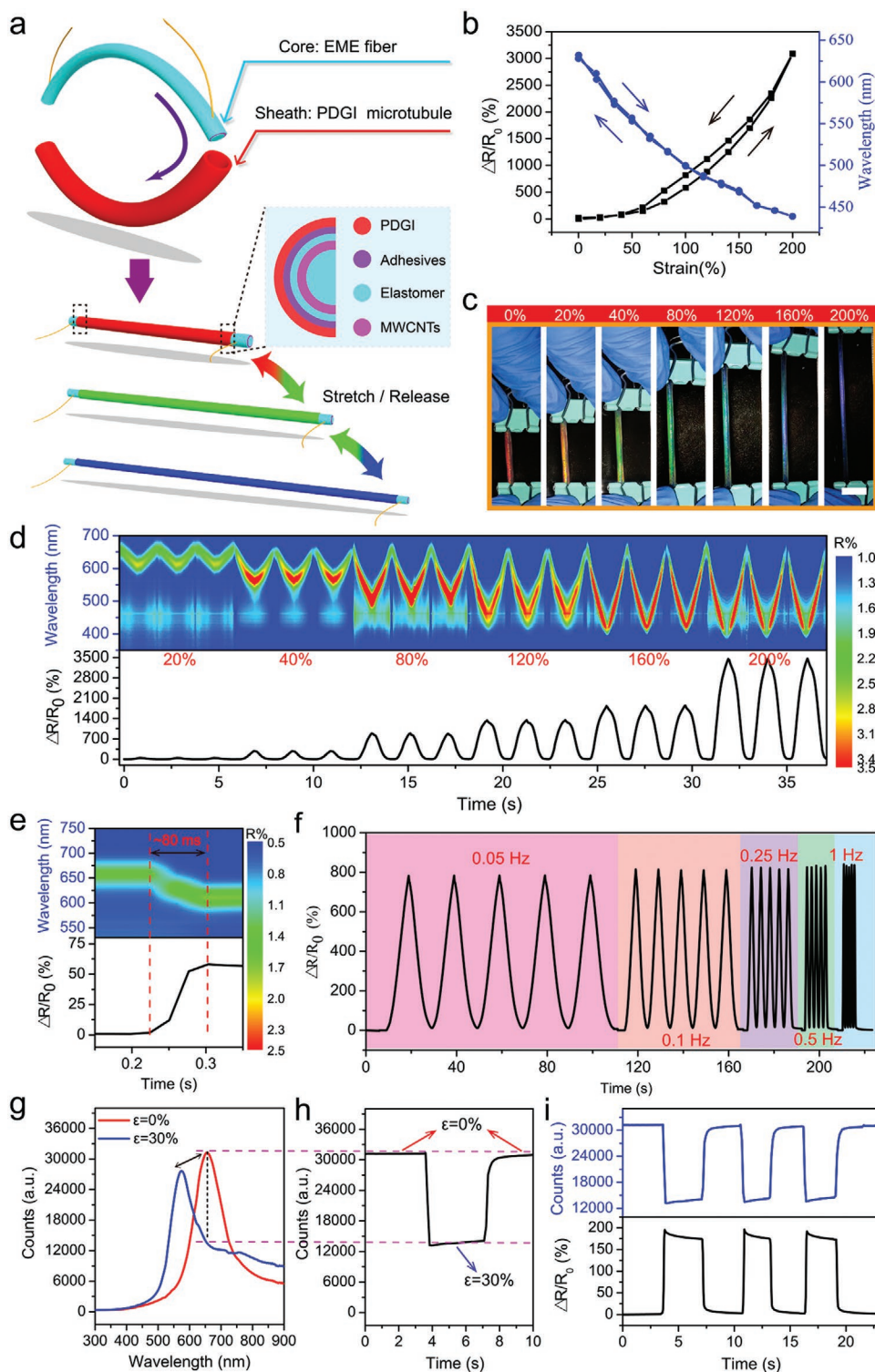


Figure 4. a) Schematic diagram showing the fabrication of interactive full-color changeable multisheath interactive fiber strain sensor. b) Relative resistance and the reflection wavelength curves as a function of strain under cyclic stretching/releasing up to 200% strain. c) Optical images of the sensor under different strains. Scale bar is 1 cm. d) Changes of relative resistance and reflection peak wavelength under different strains of 20%, 40%, 80%, 120%, 160%, and 200% at a frequency of 0.5 Hz. e) Response time measurement for electrical and optical signals of the sensor applied strain from 0% to 20%. f) Curves of relative resistance as a function of time with 100% strain at frequencies of 0.025, 0.05, 0.1, 0.25, 0.5, and 1.0 Hz. g) Reflectance spectra of the sensor at 0% and 30% strains. h) Variation of optical intensity of initial reflection wavelength (650 nm) during stretching/releasing process. i) Curves of relative resistance and optical intensity (650 nm) as a function of time under repeated stretching/releasing with 30% strain.

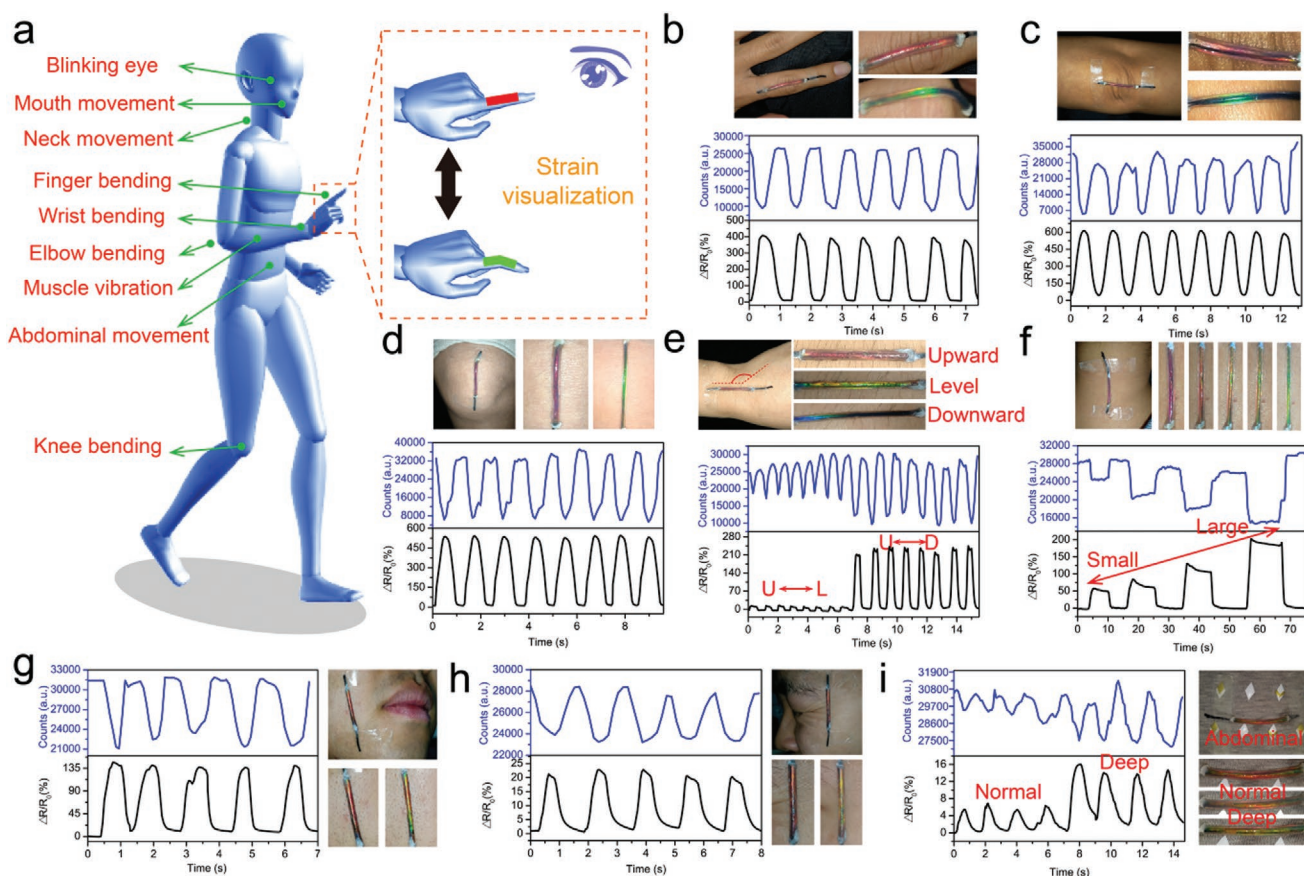


Figure 5. Changes of the electrical and optical signals of the interactive sensor when monitoring the movements of different parts of the human body, and the corresponding photographs. a) Schematic diagram of different moving parts of human body. b) Finger bending. c) Elbow bending. d) Knee bending. e) Wrist bending up and down. f) Cervical vertebrae bending of varying degrees. g) Mouth opening and closing. h) Blinking eye. i) Abdominal movements during normal and deep breathing.

promising applications in human–machine exchange, prosthesis, e-skin, health monitoring, and soft robotics.

3. Conclusion

In summary, this work demonstrates a novel interactive fiber sensor featuring full-color changes, high stretchability, high sensitivity ($GF \approx 24.2$), high resolution ($\approx 1 \text{ nm}\%^{-1}$), and rapid response for wearable electronic devices. The device was obtained via the design of a multisheath architecture composed of piezoresistive EME fiber and mechanochromic PDGI photonic microtubule, providing electrical signal and optical responses, respectively. The electrical and optical signals can be recognized by instruments and human eyes synchronously during stretching/releasing cycles for strain quantification and visualization. We reported remarkable interactive fiber sensor realizing continuous color changes across the entire visible spectrum (from 632 to 439 nm) over a large working range (0–200%) for the first time. Furthermore, compared to other interactive devices based on chromic dyes, it also exhibits a large advantage in response speed ($\approx 80 \text{ ms}$). As a proof-of-concept, we have demonstrated the interactive monitoring of both large (e.g., finger, elbow joint, and knee joint bending)

and micro (e.g., eye blinking) movements of human body with our fiber sensor. We believe that our PE strain sensor has broad application prospects in human–machine exchange, e-skin, health monitoring, and other fields. In subsequent work, by integrating the stretchable electronic sensor with multiresponsive photonic materials, various multifunctional interactive electronic devices could be fabricated to simultaneously detect and visualize a series of external stimuli, such as temperature, humidity, ions, and pH. More importantly, construction of multifunctional interactive electronic devices will be greatly simplified by further designing and utilizing single multiresponsive smart materials with photoelectric response capability.

4. Experimental Section

Materials: The nonionic surfactant DGI was purchased from Yuhao Chemical in China. AAm, MBAA, SDS, and TPO were purchased from Aladdin. Ecoflex 00-30 was purchased from Smooth-On, Inc. MWCNTs with 97% purity and 15–30 μm length were purchased from Shenzhen Tu Ling Ji Hua Ke Ji Co., Ltd. in China.

Preparation of PDGI Hydrogel Precursor Solution: First, DGI (140 mg) was added to deionized water (5 mL) containing AAm (720 mg), MBAA (2–16 mg), SDS (0.14 mg), and TPO (3.5 mg). Then, the solution was placed in an electric blast drying box at 50 $^{\circ}\text{C}$ and allowed to stand for 24 h until the DGI lamellar bilayer structure was formed. The higher the

content of MBAA in solution was, the smaller the photonic bandgap of the PDGI hydrogel after UV curing, as shown in Figure S2 and Table S1 in the Supporting Information.

Preparation of the PDGI Photonic Crystal Gel Microtubule: The fabrication process of PDGI microtubule is depicted in Figure 2a. To fabricate the PDGI microtubule, a Teflon tube and a Teflon fiber were used as template. First, PDGI precursor solution was injected into a transparent Teflon tube template by a syringe (Figure 2a_{1,a2}). Then, a Teflon fiber was inserted into the middle of the tube and the fiber was fixed at both ends of the tube with a ring washer. Next, the solution was cured into the hydrogel with a 365 nm ultraviolet lamp (12 W) at ≈50 °C for 5 min (Figure 2a₃). Due to the hydrophobic properties of the Teflon material, the PDGI microtubule could be manually separated from the mold, and then immersed in deionized water for 1 day to reach swelling equilibrium (Figure 2a₄). PDGI microtubules with different diameters and wall thicknesses were prepared by changing the size of the template. A series of red, orange, green, and blue PDGI microtubules were prepared with 2.0 mm × 0.9 mm, 2.0 mm × 0.5 mm, 1.5 mm × 0.5 mm, and 1.5 mm × 0.9 mm (tube diameter × fiber diameter) templates, respectively.

Preparation of Ecoflex Fiber: Parts A and B (mass ratio 1:1) of Ecoflex 00-30 were mixed and stirred for 5 min. The mixture was injected into a polyvinyl chloride (PVC) tube with an inner diameter of 1 mm by a syringe, and cured at room temperature for 4 h. After that, it was soaked in chloroform solution for 20 min. The PVC tube and Ecoflex fiber were separated due to their different degrees of swelling. The Ecoflex fiber was placed in the air for 10 min to make it deswell and was left for later use.

Preparation of EME Fiber: First, MWCNTs were dispersed in chloroform solvent to prepare MWCNTs dispersion solutions with different mass fractions (1%, 1.5%, and 2%), and then the MWCNTs were uniformly dispersed in solvents by ultrasonic vibration for 2 h in a sealed glass bottle. Second, the Ecoflex fiber was soaked in chloroform solvent for 30 min for swelling. After that, the swollen fiber was soaked in MWCNTs dispersion solution for 5 s and then immediately removed to obtain a MWCNTs/Ecoflex (ME) fiber. To obtain ME fibers with different MWCNT loads, the fibers could be dipped for different numbers of cycles (1–3 cycles) in the MWCNTs dispersion solution. Third, the ME fiber was suspended in air for 20 min for deswelling. Next, copper wires were tied to both ends of the fiber as conductive channels (Figure S6, Supporting Information). Finally, Ecoflex 00-30 solution was coated on the surface of the ME fiber by dipping and then was hung vertically. Under the effect of gravity, Ecoflex 00-30 solution was evenly distributed on the fiber surface. After 4 h of curing, Ecoflex/MWCNTs/Ecoflex (EME) fiber was obtained.

Preparation of PE Sensor: EME fiber prepared with 3 dip-coating cycles in a 2 wt% MWCNTs dispersion and PDGI photonic crystal microtubule were selected as electrical and optical materials, respectively. The above EME fiber was inserted into the PDGI microtubule, followed by adhering with ethyl cyanoacrylate adhesive at both ends of the sensor. To ensure close contact and thus the synchronous change in optical and electrical signals, the diameter of the EME fiber equals the inner diameter of the PDGI microtubule.

Characterization: SEM images were obtained by a Nova NanoSEM 450. The cross-sections of hydrogels were imaged using a metallographic microscope (MIT300/500, Cnoptec). The normal-incidence optical reflection spectrum and the changes in light reflection intensity at a specified wavelength were obtained using a PG2000-pro fiber optic spectrometer with a tungsten halogen light source (Shanghai Ideo Optics Corp., Ltd.). The resistance test was performed using a Digital Multimeter (Keysight 3440A/11A Digital Multimeter (Agilent)). Mechanical tensile test was carried out by a universe testing machine (PT-305, Dongguan Precise-Test Equipment Co., Ltd.). The repeated stretching and releasing behavior of the sensor was controlled by a homemade cyclic tensile tester with adjustable frequency. When applied to human motion monitoring, the sensor was fixed on various parts of human body with tape, and the resistance was monitored in real time with a digital multimeter. A spectrometer was used to monitor the light intensity at the specified wavelength in real time. During the monitoring process, the vertical distance between the spectrometer probe and the

moving part remained unchanged. Informed consent was obtained from the volunteer who participated in the experiments.

Supporting Information

Supporting Information is available from the Wiley Online Library or from the author.

Acknowledgements

The work was financially supported by the Key Program of National Natural Science Foundation of China (21536002), the National Natural Science Foundation of China (21506023), the National Science Foundation of Liaoning Province (20180550501), the fund for innovative research groups of the National Natural Science Fund Committee of Science (21421005), and the Fundamental Research Funds for the Central Universities (DUT19JC14 and DUT2019TA06).

Conflict of Interest

The authors declare no conflict of interest.

Keywords

hydrogel, interactive sensing, photonic microtubules, stretchable electronics, structural color

Received: January 14, 2020

Revised: February 17, 2020

Published online: March 13, 2020

- [1] a) J. Park, Y. Lee, J. Hong, M. Ha, Y. D. Jung, H. Lim, S. Y. Kim, H. Ko, *ACS Nano* **2014**, *8*, 4689; b) S. Gong, W. Schwalb, Y. Wang, Y. Chen, Y. Tang, J. Si, B. Shirinzadeh, W. Cheng, *Nat. Commun.* **2014**, *5*, 3132.
- [2] a) J. Y. Sun, C. Keplinger, G. M. Whitesides, Z. Suo, *Adv. Mater.* **2014**, *26*, 7608; b) R. Z. Li, A. Hu, T. Zhang, K. D. Oakes, *ACS Appl. Mater. Interfaces* **2014**, *6*, 21721.
- [3] a) C. F. Pan, L. Dong, G. Zhu, S. M. Niu, R. M. Yu, Q. Yang, Y. Liu, Z. L. Wang, *Nat. Photonics* **2013**, *7*, 752; b) W. Z. Wu, X. N. Wen, Z. L. Wang, *Science* **2013**, *340*, 952; c) X. Pu, M. M. Liu, X. Y. Chen, J. M. Sun, C. H. Du, Y. Zhang, J. Y. Zhai, W. G. Hu, Z. L. Wang, *Sci. Adv.* **2017**, *3*, e1700015.
- [4] a) C. Wang, C. Wang, Z. Huang, S. Xu, *Adv. Mater.* **2018**, *30*, 1801368; b) S. T. Han, H. Peng, Q. Sun, S. Venkatesh, K. S. Chung, S. C. Lau, Y. Zhou, V. A. L. Roy, *Adv. Mater.* **2017**, *29*, 1700375.
- [5] a) G. Kim, S. Cho, K. Chang, W. S. Kim, H. Kang, S. P. Ryu, J. Myoung, J. Park, C. Park, W. Shim, *Adv. Mater.* **2017**, *29*, 1606120; b) L. Zhang, M. Liao, L. Bao, X. Sun, H. Peng, *Small Methods* **2017**, *1*, 1700211.
- [6] a) C. Wang, D. Hwang, Z. B. Yu, K. Takei, J. Park, T. Chen, B. W. Ma, A. Javey, *Nat. Mater.* **2013**, *12*, 899; b) E. H. Kim, S. H. Cho, J. H. Lee, B. Jeong, R. H. Kim, S. Yu, T. W. Lee, W. Shim, C. Park, *Nat. Commun.* **2017**, *8*, 14964; c) Y. C. Lai, B. W. Ye, C. F. Lu, C. T. Chen, M. H. Jao, W. F. Su, W. Y. Hung, T. Y. Lin, Y. F. Chen, *Adv. Funct. Mater.* **2016**, *26*, 1286.
- [7] T. Yokota, P. Zalar, M. Kaltenbrunner, H. Jinno, N. Matsuhisa, H. Kitanosako, Y. Tachibana, W. Yukita, M. Koizumi, T. Someya, *Sci. Adv.* **2016**, *2*, e1501856.

- [8] a) C. Larson, B. Peele, S. Li, S. Robinson, M. Totaro, L. Beccai, B. Mazzolai, R. Shepherd, *Science* **2016**, 351, 1071; b) E. H. Kim, H. Han, S. Yu, C. Park, G. Kim, B. Jeong, S. W. Lee, J. S. Kim, S. Lee, J. Kim, J. U. Park, W. Shim, C. Park, *Adv. Sci.* **2019**, 6, 1802351; c) X. Wang, M. Que, M. Chen, X. Han, X. Li, C. Pan, Z. Wang, *Adv. Mater.* **2017**, 29, 1605817; d) A. Yakoh, R. Alvarez-Diduk, O. Chailapakul, A. Merkoci, *ACS Appl. Mater. Interfaces* **2018**, 10, 20775.
- [9] H. H. Chou, A. Nguyen, A. Chortos, J. W. F. To, C. Lu, J. G. Mei, T. Kurosawa, W. G. Bae, J. B. H. Tok, Z. A. Bao, *Nat. Commun.* **2015**, 6, 8011.
- [10] a) S. Zeng, H. Sun, C. Park, M. Zhang, M. Zhu, M. Yan, N. Chov, E. Li, A. T. Smith, G. Xu, S. Li, Z. Hou, Y. Li, B. Wang, D. Zhang, L. Sun, *Mater. Horiz.* **2020**, 7, 164; b) C. J. Yu, Y. H. Li, X. Zhang, X. Huang, V. Malyarchuk, S. D. Wang, Y. Shi, L. Gao, Y. W. Su, Y. H. Zhang, H. X. Xu, R. T. Hanlon, Y. G. Huang, J. A. Rogers, *Proc. Natl. Acad. Sci. USA* **2014**, 111, 12998.
- [11] J. Park, Y. Lee, M. H. Barbee, S. Cho, S. Cho, R. Shanker, J. Kim, J. Myoung, M. P. Kim, C. Baig, S. L. Craig, H. Ko, *Adv. Mater.* **2019**, 31, 1808148.
- [12] J. Teyssier, S. V. Saenko, D. van der Marel, M. C. Milinkovitch, *Nat. Commun.* **2015**, 6, 6368.
- [13] M. Qin, M. Sun, R. Bai, Y. Mao, X. Qian, D. Sikka, Y. Zhao, H. J. Qi, Z. Suo, X. He, *Adv. Mater.* **2018**, 30, 1800468.
- [14] L. M. Mäthger, S. L. Senft, M. Gao, S. Karaveli, G. R. R. Bell, R. Zia, A. M. Kuzirian, P. B. Dennis, W. J. Crookes-Goodson, R. R. Naik, G. W. Kattawar, R. T. Hanlon, *Adv. Funct. Mater.* **2013**, 23, 3980.
- [15] Y. Yue, T. Kurokawa, M. A. Haque, T. Nakajima, T. Nonoyama, X. Li, I. Kajiwara, J. P. Gong, *Nat. Commun.* **2014**, 5, 4659.
- [16] H. B. Seo, S. Y. Lee, *Sci. Rep.* **2017**, 7, 44927.
- [17] S. A. Morin, R. F. Shepherd, S. W. Kwok, A. A. Stokes, A. Nemiroski, G. M. Whitesides, *Science* **2012**, 337, 828.
- [18] F. Liu, B. Q. Dong, X. H. Liu, Y. M. Zheng, J. Zi, *Opt. Express* **2009**, 17, 16183.
- [19] a) Y. Fang, Y. Ni, S. Y. Leo, C. Taylor, V. Basile, P. Jiang, *Nat. Commun.* **2015**, 6, 7416; b) W. Lu, H. Li, B. Huo, Z. Meng, M. Xue, L. Qiu, S. Ma, Z. Yan, C. Piao, X. Ma, *Sens. Actuators, B* **2016**, 234, 527; c) T. H. Park, S. Yu, S. H. Cho, H. S. Kang, Y. Kim, M. J. Kim, H. Eoh, C. Park, B. Jeong, S. W. Lee, D. Y. Ryu, J. Huh, C. Park, *NPG Asia Mater.* **2018**, 10, 328; d) P. Snapp, P. Kang, J. Leem, S. Nam, *Adv. Funct. Mater.* **2019**, 29, 1902216.
- [20] a) I. B. Burgess, N. Koay, K. P. Raymond, M. Kolle, M. Loncar, J. Aizenberg, *ACS Nano* **2012**, 6, 1427; b) Y. Zhang, Q. Fu, J. Ge, *Nat. Commun.* **2015**, 6, 7510; c) H. S. Lim, J. H. Lee, J. J. Walsh, E. L. Thomas, *ACS Nano* **2012**, 6, 8933; d) H. Xu, Y. F. Lu, J. X. Xiang, M. K. Zhang, Y. J. Zhao, Z. Y. Xie, Z. Z. Gu, *Nanoscale* **2018**, 10, 2090.
- [21] a) K. Matsubara, M. Watanabe, Y. Takeoka, *Angew. Chem.* **2007**, 119, 1718; b) M. C. Chiappelli, R. C. Hayward, *Adv. Mater.* **2012**, 24, 6100.
- [22] a) G. Z. Han, Z. Y. Xie, D. Zheng, L. G. Sun, Z. Z. Gu, *Appl. Phys. Lett.* **2007**, 91, 141114; b) Z. Y. Xie, L. G. Sun, G. Z. Han, Z. Z. Gu, *Adv. Mater.* **2008**, 20, 3601.
- [23] H. Tan, Q. Lyu, Z. Xie, M. Li, K. Wang, K. Wang, B. Xiong, L. Zhang, J. Zhu, *Adv. Mater.* **2019**, 31, e1805496.
- [24] a) M. Hayakawa, T. Onda, T. Tanaka, K. Tsujii, *Langmuir* **1997**, 13, 3595; b) M. A. Haque, G. Kamita, T. Kurokawa, K. Tsujii, J. P. Gong, *Adv. Mater.* **2010**, 22, 5110; c) K. Naitoh, Y. Ishii, K. Tsujii, *J. Phys. Chem.* **1991**, 95, 7915; d) M. Ilyas, M. A. Haque, Y. Yue, T. Kurokawa, T. Nakajima, T. Nonoyama, J. P. Gong, *Macromolecules* **2017**, 50, 8169.
- [25] M. A. Haque, T. Kurokawa, J. P. Gong, *Soft Matter* **2012**, 8, 8008.
- [26] a) M. A. Haque, T. Kurokawa, G. Kamita, J. P. Gong, *Macromolecules* **2011**, 44, 8916; b) X. F. Li, T. Kurokawa, R. Takahashi, M. A. Haque, Y. F. Yue, T. Nakajima, J. P. Gong, *Macromolecules* **2015**, 48, 2277.
- [27] Y. Yue, X. Li, T. Kurokawa, M. Anamul Haque, J. P. Gong, *J. Mater. Chem. B* **2016**, 4, 4104.
- [28] M. A. Haque, K. Mito, T. Kurokawa, T. Nakajima, T. Nonoyama, M. Ilyas, J. P. Gong, *ACS Omega* **2018**, 3, 55.
- [29] Y. F. Yue, M. A. Haque, T. Kurokawa, T. Nakajima, J. P. Gong, *Adv. Mater.* **2013**, 25, 3106.
- [30] J. Y. Sun, X. Zhao, W. R. Illeperuma, O. Chaudhuri, K. H. Oh, D. J. Mooney, J. J. Vlassak, Z. Suo, *Nature* **2012**, 489, 133.
- [31] R. S. Wong, M. Ashton, K. Dodou, *Pharmaceutics* **2015**, 7, 305.
- [32] S. J. Park, J. Kim, M. Chu, M. Khine, *Adv. Mater. Technol.* **2016**, 1, 1600053.
- [33] a) Y. Cheng, R. Wang, J. Sun, L. Gao, *Adv. Mater.* **2015**, 27, 7365; b) M. Amjadi, A. Pichitpajongkit, S. Lee, S. Ryu, I. Park, *ACS Nano* **2014**, 8, 5154.
- [34] T. S. Natarajan, S. B. Eshwaran, K. W. Stockelhuber, S. Wiessner, P. Potschke, G. Heinrich, A. Das, *ACS Appl. Mater. Interfaces* **2017**, 9, 4860.
- [35] a) Z. H. Tang, S. H. Jia, F. Wang, C. S. Bian, Y. Y. Chen, Y. L. Wang, B. Li, *ACS Appl. Mater. Interfaces* **2018**, 10, 6624; b) J. H. Ma, P. Wang, H. Y. Chen, S. J. Bao, W. Chen, H. B. Lu, *ACS Appl. Mater. Interfaces* **2019**, 11, 8527; c) S. W. Lee, J. J. Park, B. H. Park, S. C. Mun, Y. T. Park, K. Liao, T. S. Seo, W. J. Hyun, O. O. Park, *ACS Appl. Mater. Interfaces* **2017**, 9, 11176.
- [36] J. Lee, M. Lim, J. Yoon, M. S. Kim, B. Choi, D. M. Kim, D. H. Kim, I. Park, S. J. Choi, *ACS Appl. Mater. Interfaces* **2017**, 9, 26279.
- [37] W. Thongruang, C. M. Balik, R. J. Spontak, *J. Polym. Sci., Part B: Polym. Phys.* **2002**, 40, 1013.